Applied Bionics and Biomechanics
Vol. 6, No. 2, June 2009, 127–142

Taylor & Francis
Taylor & Francis Group

ARMin III – arm therapy exoskeleton with an ergonomic shoulder actuation

Tobias Nef[a,b*], Marco Guidali[c,d] and Robert Riener[c,d]

[a] *Department of Biomedical Engineering, The Catholic University of America, Washington, DC, USA;* [b] *Center for Applied Biomechanics and Rehabilitation Research, National Rehabilitation Hospital, Washington, DC, USA;* [c] *Spinal Cord Injury Center, Balgrist University Hospital, University Zurich, Switzerland;* [d] *Sensory-Motor Systems Lab, Institute of Robotics and Intelligent Systems, ETH Zurich, Switzerland*

(*Received 7 October 2008; final version received 22 February 2009*)

Rehabilitation robots have become important tools in stroke rehabilitation. Compared to manual arm training, robot-supported training can be more intensive, of longer duration and more repetitive. Therefore, robots have the potential to improve the rehabilitation process in stroke patients. Whereas a majority of previous work in upper limb rehabilitation robotics has focused on end-effector-based robots, a shift towards exoskeleton robots is taking place because they offer a better guidance of the human arm, especially for movements with a large range of motion. However, the implementation of an exoskeleton device introduces the challenge of reproducing the motion of the human shoulder, which is one of the most complex joints of the body. Thus, this paper starts with describing a simplified model of the human shoulder. On the basis of that model, a new ergonomic shoulder actuation principle that provides motion of the humerus head is proposed, and its implementation in the ARMin III arm therapy robot is described. The focus lies on the mechanics and actuation principle. The ARMin III robot provides three actuated degrees of freedom for the shoulder and one for the elbow joint. An additional module provides actuated lower arm pro/supination and wrist flexion/extension. Five ARMin III devices have been manufactured and they are currently undergoing clinical evaluation in hospitals in Switzerland and in the United States.

Keywords: arm rehabilitation robotics; exoskeleton; shoulder actuation

1. Introduction

1.1. Clinical background

Stroke is the neurological disease with the highest prevalence and it is the leading cause of disability. Recent studies estimate that it affects more than 1 million people in the EU (Thorvaldsen et al. 1995; Brainin et al. 2000) and more than 0.7 million in the United States each year (Rosamond et al. 2007). One major symptom of stroke is acute hemiparesis that affects the upper extremities. Several studies show that sensorimotor arm therapy has positive effects on the rehabilitation progress of stroke patients (see Platz 2003 for review). The goal hereby is to induce long-term brain plasticity and improve functional outcomes. The critical factors of treatment are that the therapy is *intensive* (Kwakkel et al. 1999), *of long duration* (Sunderland et al. 1992), *repetitive* (Butefisch et al. 1995) and *task-oriented* (Bayona et al. 2005).

Regarding these criteria, one-to-one manually assisted arm training has several limitations. The training is labour-intensive and, therefore, expensive. The disadvantageous consequence is that the rehabilitation period and the single training sessions are often shorter than required to gain a maximal therapeutic outcome. Furthermore, manually assisted training lacks repeatability and objective measures of patient performance and progress.

1.2. Robots in rehabilitation

Introducing robotics can overcome some shortcomings of manually assisted arm training. Thus, a part of the training session can be automated and the duration and the number of the training sessions can be increased. It is, furthermore, hypothesised that the use of patient-cooperative controllers that support the patient only as much as needed can increase the participation of the patient and, therefore, the intensity of training (Riener and Fuhr 1998; Riener et al. 2005a; Nef et al. 2007a). While it is easy for a rehabilitation robot to deliver repetitive training, it is challenging to provide task-oriented movements. These tasks should be based on activities of daily living (ADL) and include eating, drinking, dressing and other important activities. They require robots with many degrees of freedom (DOF) supporting 3D movement of the whole arm and the hand (van Andel et al. 2008).

Several groups have developed and evaluated arm therapy robots (see Volpe et al. 2001; Riener et al. 2005b; Kahn et al. 2006; Prange et al. 2006; Kwakkel et al. 2008 for

*Corresponding author. Email: tobiasnef@gmail.com

ISSN: 1176-2322 print / 1754-2103 online

DOI: 10.1080/11762320902840179
http://www.informaworld.com

review). Most of the existing arm therapy robots are either end-effector-based or exoskeletons.

End-effector-based robots are connected with the patient's hand or forearm at one point. Depending on the available DOF of the robot, the human arm can be positioned and/or oriented in space. The robot's rotation axes generally do not correspond with the human joint rotation axes. That is why, from a mechanical point of view, these robots are easier to produce and to use. Many research groups have developed end-effector-based robots. The MIT Manus (Krebs et al. 2004), the Assisted Rehabilitation and Measurement Guide (Reinkensmeyer et al. 2000), the Mirror Image Motion Enabler (Lum et al. 2004), the Bi-Manu-Track (Hesse et al. 2005), the GENTLE/s (Cote et al. 2003), the Neurorehabilitation Robot (Fanin et al. 2003) and the Arm Coordination Training Robot (Dewald et al. 2004) are examples of current end-effector-based robotic therapy devices.

An important advantage of end-effector-based robots is that they are easy to adjust to different arm lengths. A disadvantage is that, in general, the arm posture and/or the individual joint interaction torques are not fully determined by the robot. This is because the patient and the robot interact just through one point, which is the robot's end-effector. A consequence is that the range of motion (ROM) of end-effector-based robots is limited, and in general exoskeleton robots are better suited to train activities that require a large ROM.

1.3. Rehabilitation exoskeletons

The mechanical structure of exoskeletons resembles human arm anatomy, and the robot's rotation axes correspond with that of human arms. Consequently, the human arm can be attached to the exoskeleton at several points. Adaptation to different body sizes is therefore more difficult than in end-effector-based systems, because each robot link must be adjusted to the corresponding patient arm segment length. However, the advantage of an exoskeleton robot compared to an end-effector-based system is that the arm posture is fully determined. Torques applied to each joint of the human arm can be controlled separately and hyperextension of the individual joints, i.e. the elbow joint, can be avoided by mechanical end stops. Thus, this provides larger ranges of movements, as required to perform several ADL tasks. The possibility to control the interacting torques in each joint separately is essential, e.g. when the subjects' elbow flexors are spastic. The mobilisation of the elbow joint must not induce reaction torques and forces in the shoulder joint, which can be guaranteed by an exoskeleton robot, but not by an end-effector-based one. This is important because the hemiparetic shoulder is an instable joint (Zatsiorsky 1998). That is why therapists use both hands to mobilise a spastic elbow joint. In order to avoid exercising forces to the shoulder, one hand holds the lower arm while the other hand holds the upper arm. This is comparable to an exoskeleton robot with a cuff fixed to the lower and another fixed to the upper arm.

Some examples of passive, i.e. non-motorised, arm rehabilitation exoskeletons are the Dampace (Stienen et al. 2007) and the Armeo (Sanchez et al. 2006). The MGA-Exoskeleton (Carignan and Liszka 2005), the L-Exos (Bergamasco et al. 2007), Rosen's arm robot (Rosen et al. 2005), The Intelligent Robotic Arm (Zhang et al. 2007) and the ARMin I and II (Nef et al. 2007a) are active, i.e. motorised devices.

The requirement that the robot's rotation axes must correspond with the human rotation axes is easy to fulfill for simple joints like the elbow joint, but difficult for complex joints like the shoulder joint. A common oversimplification that can lead to misalignment between the robot and the human is the definition of a 'ball and socket type' joint for describing the movement of the human shoulder. While this assumption nearly holds for small angles exerted or exclusive glenohumeral motion, it significantly deviates for larger motions (Schiele and van der Helm 2006).

As shown in Figure 1, during arm elevation movement, vertical translational motion of the humerus head (HH) occurs. This implies that the human bone undergoes translational movements in addition to the three predominant rotational movements.

There are different strategies of how to deal with this additional translation movement. One strategy is to add one (Armeo), two (ARMin I) or three (Dampace) passive joints to the three dominant rotational joints so that the exoskeleton can compensate for HH translation movement and autoalign with the human skeleton. The Dampace shoulder has the obligatory three rotational joints plus three additional translational joints to ensure that the exoskeleton aligns with the human skeleton, and pure torque is applied to the human shoulder joint.

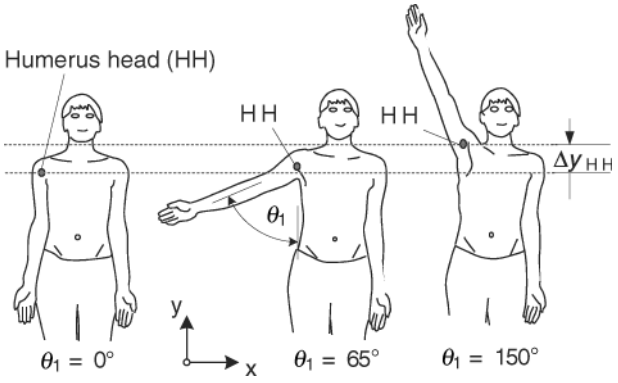

Figure 1. Location of the humerus head for three different arm elevation angles ($\theta_1 = 0°$; $\theta_1 = 65°$; $\theta_1 = 150°$) in the frontal plane (*xy*-plane). During arm elevation from $\theta_1 = 0°$ to 150°, the humerus head undergoes a vertical translation movement with the magnitude Δy_{HH}.

Adding passive joints to an actuated exoskeleton results in loss of statical determination of the robot. This adds more freedom to the patient's limb but also reduces guidance and mechanical support of the limb. In case of the ARMin I device, this was problematic for stroke subjects with unstable shoulder joints, e.g. resulting from shoulder subluxations (Nef et al. 2007a). However, these findings are robot-specific and do not apply to other devices.

Another strategy that has been used for the ARMin II device is to add a translational joint to the robot's shoulder actuation (Mihelj et al. 2007a). The translational joint is mechanically coupled to the arm elevation angle θ_1 (Figure 1) and compensates for vertical translational movement of the HH. This motion can also be achieved by adding a fourth motorised rotational joint to the shoulder actuation. In the case of the MGA-Exoskeleton, this results in a statically determined shoulder actuation that can compensate for translational movement of the HH. The advantage is that the compensation strategy is flexible as it can be adjusted by the software. The disadvantage is the added complexity.

This paper starts with a quantitative description of the human shoulder movement. The model describes the translation movement of the HH during arm elevation. On the basis of this model, a new shoulder actuation principle is developed and evaluated. The paper finally presents the mechanics and actuation of the ARMin III robot that comprises the new shoulder actuation principle.

The control strategies used for the patient-cooperative control of the ARMin robots are not presented in this paper. Information can be found in Oldewurtel et al. (2007), Mihelj et al. (2007b), Nef et al. (2007b), and Nef and Lum (2009).

2. Methods

2.1. Specifications

The training of ADL includes tasks like eating, drinking, combing hair, etc. For most of these ADL tasks, the hand has to reach a point in space, grasp an object and then control the position and orientation of the object until the task is completed. Therefore, the robot must be able to support movements of the shoulder (3 DOF), the elbow (1 DOF), the lower arm (1 DOF) and the wrist (1 DOF). This paper focuses on the shoulder and elbow actuation of the robot ($3 + 1$ DOF). A lower arm module with two additional DOFs for lower arm pro/supination and wrist flexion/extension can be connected to the device.

The ROM of the robot must match that of the human arm as closely as possible (Winter et al. 1989). In order to obtain satisfactory control performance of patient-cooperative control strategies, which are based on impedance and admittance architectures, the robot should have low friction and negligible backlash. Furthermore, the motor/gear units should be backdrivable. Passive backdrivability helps to achieve good performance of the impedance controller (Krebs et al. 2004) and it is a desirable safety feature of exoskeleton robots that helps to release the patient in the case of power loss or in the case of therapist-triggered cut-off.

The required velocities and accelerations (Table 1) have been determined by measuring the movements of a healthy subject during ADL tasks (Nef et al. 2007a). These values served as inputs for a simple dynamic model applied to estimate the required joint torques. In order to ensure that the robot will be strong enough to overcome resistance from the human due to spasms and other complications that are difficult to model, rather high values have been selected. The required end-point payload is 3 kg, which allows simulating the manipulation of heavier objects.

It is required that the robot is easy to handle and that safety is always guaranteed for both patient and therapist. Furthermore, it must be possible to use the device either for the right or the left arm.

2.2. The human shoulder

The humerus bone connects to the scapula through the glenohumeral joint, the scapula connects to the clavicle via the acromioclavicular joint and the clavicle connects to the thorax via the sternoclavicular joint (Figure 2). Elevation of the humerus results from rotations of the humerus around the glenohumeral joint, from rotations of the scapula around the acromioclavicular joint and from rotations of the clavicle around the sternoclavicular joint. Through this mechanism, translational movement of the HH occurs. Since the exoskeleton robot is fixed to the upper arm via cuffs, the motion of the HH should be known. This is because the robot must stay aligned with the human limb, and, therefore, follow the natural motion of the humerus.

Numerous groups have analysed human shoulder movements with imaging techniques (Freedmann and Munro 1966; Doody et al. 1970; Soslowsky et al. 1992) and with non-invasive motion recording techniques (Baag and

Table 1. Requirements for the range of motion (ROM), velocity and the maximal torques.

	ROM	Velocity (°/s)	Acceleration (°/s^2)	Torque (Nm)
Axis 1 – Arm elevation: θ_1	45°–135°	71	103	20
Axis 2 – Plane of elevation: θ_2	−45°–135°	60	129	20
Axis 3 – Internal/external shoulder rotation: θ_3	−90°–90°	150	245	20
Axis 4 – Elbow flexion/extension: θ_4	0°–120°	91	116	20

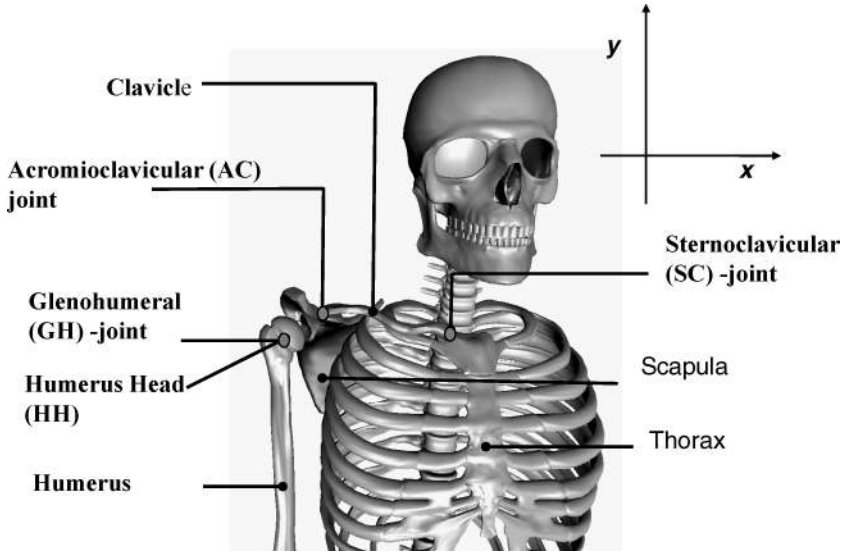

Figure 2. Human shoulder joint.

Forrest 1988; Culham and Peat 1993; van der Helm and Pronk 1995; De Groot et al. 1999; Lenarcic and Stanisic 2003). The shoulder analysis in this paper is based on a methodology introduced by Moeslund et al. (2005), which allows to simplify and quantify human shoulder movement. The purpose of this analysis is to derive a simplified model of the coupling between the arm elevation angle and the horizontal displacement of the human arm. This requires several assumptions and the aim here is to present a model that can be used for the design of the shoulder actuation mechanism.

A quantitative description of the human shoulder girdle motion is far from simple (Zatsiorsky 1998). The movement patterns of single bones differ among individuals and may be influenced by conscious control, learning and training (Lenarcic and Stanisic 2003). In order to develop a simplified quantitative description of the HH motion, the following assumptions/simplifications were made:

- Individuals with the same body size have the same HH motion.
- Training and age do not influence the HH movement pattern.

This allows expression of the relation between the position of the HH as a function of the three humerus pointing angles (θ_1 arm elevation angle (Figures 1 and 8), θ_2 angle of the plane of elevation, θ_3 internal/external shoulder rotation (Figure 8)), the body size h and the additional external mass m_{ext} which the human arm carries, as

$$\begin{pmatrix} x_{\text{HH}} \\ y_{\text{HH}} \\ z_{\text{HH}} \end{pmatrix} = \begin{pmatrix} f(\theta_1, \theta_2, \theta_3, h, m_{\text{ext}}) \\ g(\theta_1, \theta_2, \theta_3, h, m_{\text{ext}}) \\ h(\theta_1, \theta_2, \theta_3, h, m_{\text{ext}}) \end{pmatrix}. \tag{1}$$

Furthermore, the following assumptions/simplifications were made:

a. The additional external mass m_{ext} does not affect the position of the scapula nor the position of the HH (De Groot et al. 1999).
b. The pointing angle θ_3 (internal/external shoulder rotation) does not affect the position of the HH (Moeslund et al. 2005).
c. The relative movement of the HH is independent from the angle of the plane of elevation θ_2 (Zatsiorsky 1998).
d. The bone segment lengths are proportional to the body size (Cheng et al. 1998).

Taking into account assumptions a, b and c, Equation (1) can be simplified to

$$\begin{pmatrix} x_{\text{HH}} \\ y_{\text{HH}} \\ z_{\text{HH}} \end{pmatrix} = \begin{pmatrix} f(\theta_1, h) \\ g(\theta_1, h) \\ h(\theta_1, h) \end{pmatrix}. \tag{2}$$

For arm elevations in the frontal plane ($\theta_2 = 0^\circ$) it is $z_{HH} = 0$. Furthermore, assumption d allows formulation of the influence of the body size as a linear scaling factor. Thus, Equation (2) becomes

$$\begin{pmatrix} x_{\text{HH}} \\ y_{\text{HH}} \end{pmatrix} = \begin{pmatrix} f(\theta_1) \\ g(\theta_1) \end{pmatrix} \frac{h}{h_{\text{ref}}}, \tag{3}$$

where h is the subject's body size and $h_{\text{ref}} = 170$ cm is the body size from a reference subject. In order to derive a kinematic model of the human shoulder, segmented 3D CT data of a healthy man of body size h_{ref} has been used to determine segment length, initial position and orientation.

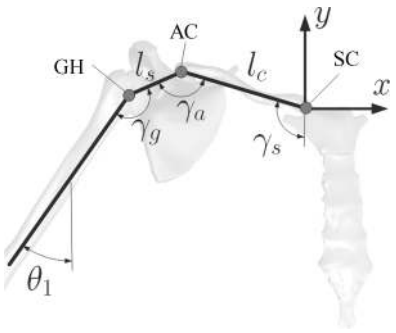

Figure 3. Joint angles of the human shoulder.

A 'ball and socket joint' is a good model for the glenohumeral joint (Solowsky et al. 1992) as well as for the acromioclavicular and the sternoclavicular joints (Moeslund et al. 2005). By introducing the angles γ_g, γ_a, γ_s, the length of the clavicle l_c and the distance between the centre of the acromioclavicular joint and the glenohumeral joint l_s (Figure 3), Equation (3) can be expressed as

$$\begin{pmatrix} x_{HH} \\ y_{HH} \end{pmatrix} = \begin{pmatrix} -l_c \cos(\hat{\gamma}_s - 90^\circ) + l_s \sin(\hat{\gamma}_a + \hat{\gamma}_s) \\ l_c \sin(\hat{\gamma}_s - 90^\circ) + l_s \cos(\hat{\gamma}_a + \hat{\gamma}_s) \end{pmatrix} \frac{h}{h_{ref}} \tag{4}$$

with

$$\hat{\gamma}_h = \gamma_{h_0} + \gamma_h(\theta_1), \quad \hat{\gamma}_a = \gamma_{a_0} + \gamma_a(\theta_1), \quad \hat{\gamma}_s = \gamma_{s_0} + \gamma_s(\theta_1). \tag{5}$$

The remaining problem is to describe the angle values $\hat{\gamma}_h, \hat{\gamma}_a, \hat{\gamma}_s$ as a function of the arm elevation angle θ_1. The initial values $\gamma_{h_0} = 118^\circ$, $\gamma_{a_0} = 143^\circ$, $\gamma_{s_0} = 99^\circ$ are measured in the CT data for the initial position with arm elevation angle $\theta_1 - 0^\circ$ ($\gamma_h(0^\circ) = \gamma_a(0^\circ) = \gamma_s(0^\circ) = 0^\circ$). From literature (Doody et al. 1970; Bagg and Forrest 1988; Culham and Peat 1993; Moeslund et al. 2005), it is known that scapula tilting is predominant for $80^\circ \leq \theta_1 \leq 140^\circ$, and that rotation in the sternoclavicular joint occurs for $0^\circ \leq \theta_1 \leq 80^\circ$ and $140^\circ \leq \theta_1 \leq 180^\circ$. Thus, the absolute angular values for some postures are known as

$$\begin{aligned} &\gamma_a(80^\circ) \approx 0^\circ, \gamma_a(140^\circ) \approx 35^\circ, \gamma_a(180^\circ) \approx 35^\circ, \\ &\gamma_s(80^\circ) \approx 15^\circ, \gamma_s(140^\circ) \approx 15^\circ, \gamma_s(180^\circ) \approx 24^\circ. \end{aligned} \tag{6}$$

In addition, it is

$$\gamma_h(\theta_1) = \theta_1 - \gamma_a(\theta_1) - \gamma_s(\theta_1). \tag{7}$$

In previous work (Nef and Riener 2008), piecewise linear functions that comply with the boundary conditions (6) have been introduced to describe the angles γ_a and γ_s as a function of θ_1. One disadvantage of this approach is that the piecewise linear functions are not continuous and that the resulting movement is not smooth. One approach that leads to smooth movements is to select a trajectory that minimises jerk (Hogan 1984). This leads to the following

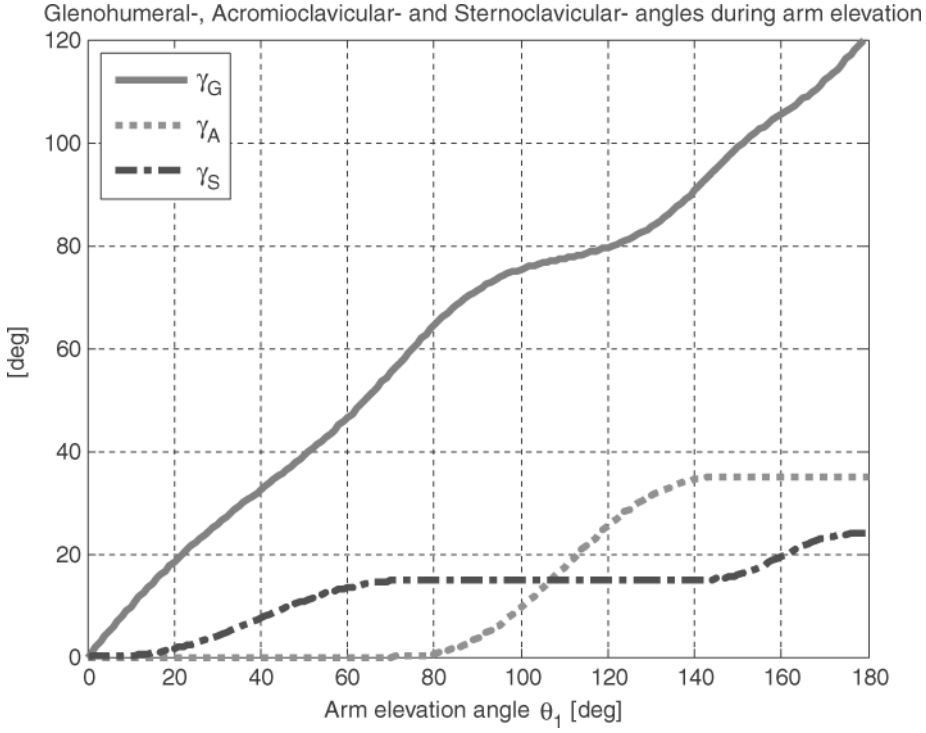

Figure 4. Angle values for an arm elevation sequence from $\theta_1 = 0^\circ - 180^\circ$.

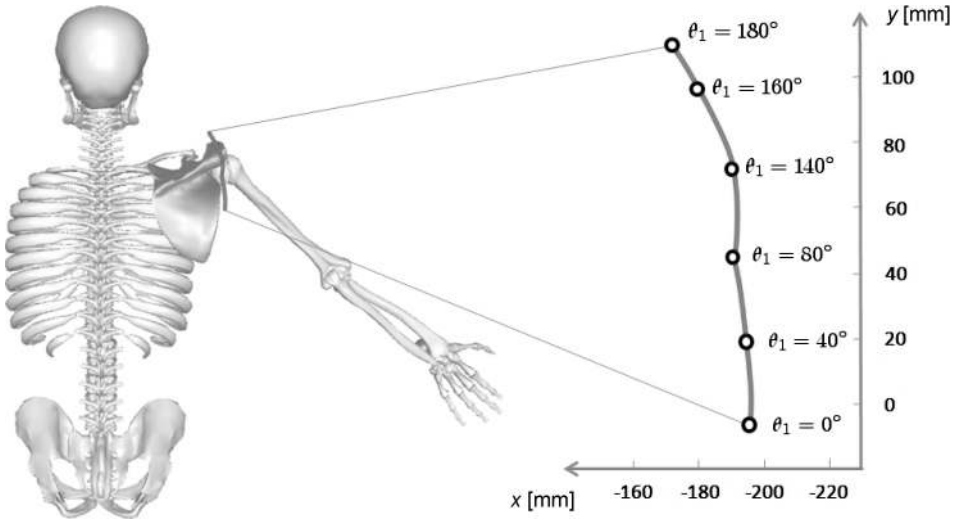

Figure 5. Back view showing the *xy*-position of the humerus head for arm elevation angles $0° \leq \theta_1 \leq 180°$ for a healthy subject of 1.7 m body size. Note that the unusual orientation of the *x*-axis is due to the back view.

trajectories:

$$\gamma_a = f(\theta_1) = \begin{cases} 0° & \text{for } 0° \leq \theta_1 < 70° \\ 35\left(10\left(\frac{\theta_1 - 70°}{140° - 70°}\right)^3 - 15\left(\frac{\theta_1 - 70°}{140° - 70°}\right)^4 + 6\left(\frac{\theta_1 - 70°}{140° - 70°}\right)^5\right) & \text{for } 70° \leq \theta_1 < 150° \\ 35° & \text{for } 150° \leq \theta_1 \leq 180° \end{cases}, \quad (8)$$

$$\gamma_b = f(\theta_1) = \begin{cases} 15\left(10\left(\frac{\theta_1}{80°}\right)^3 - 15\left(\frac{\theta_1}{80°}\right)^4 + 6\left(\frac{\theta_1}{80°}\right)^5\right) & \text{for } 0° \leq \theta_1 < 80° \\ 15° & \text{for } 80° \leq \theta_1 < 140° \\ 15° + 9\left(10\left(\frac{\theta_1 - 140°}{180° - 140°}\right)^3 - 15\left(\frac{\theta_1 - 140°}{180° - 140°}\right)^4 + 6\left(\frac{\theta_1 - 140°}{180° - 140°}\right)^5\right) & \text{for } 140° \leq \theta_1 < 180° \end{cases} \quad (9)$$

$$\gamma_h = f(\theta_1) = \theta_1 - \gamma_a(\theta_1) - \gamma_b(\theta_1). \quad (10)$$

Note that the boundary values of $\gamma_a(80°) = 0.55°$ and $\gamma_a(140°) = 34.45°$ differ slightly from the suggested values (6). This is because the boundaries in Equation (8) have been modified in order to assure that the function γ_h is strictly monotonically increasing (Figure 4).

Equation (4) and Equations (8)–(10) provide a quantitative description of the translational motion of the HH (Figure 5). Consequently, this data is used to develop and evaluate a new shoulder actuation principle.

2.3. The robotic shoulder

Once the natural movement of the HH is known (4), the aim is to find a kinematic structure that replicates this movement as closely as possible. In the ideal case, the HH motion of a healthy subject performing an arm elevation movement without the robot (HH_{WR}) should be the same motion as with the arm is connected to the exoskeleton. HH_R is defined as the position of the HH when the subject is connected to the robot. In the ideal case, we get $x_{HH_R} = x_{HH_{WR}}$ and $y_{HH_R} = y_{HH_{WR}}$ for all arm elevation angles within the ROM of the robot $\theta_{1_{min}} \leq \theta_1 \leq \theta_{1_{max}}$. The goal is to obtain a kinematics that minimises the distance between HH_R and HH_{WR}, thus minimising the cost function:

$$D_{mean} = \int_{\theta_{1_{min}}}^{\theta_{1_{max}}} \frac{1}{\theta_{1_{max}} - \theta_{1_{min}}} \left| \begin{matrix} x_{HH_{WR}}(\theta_1) - x_{HH_R}(\theta_1) \\ y_{HH_{WR}}(\theta_1) - y_{HH_R}(\theta_1) \end{matrix} \right| d\theta_1. \quad (11)$$

In previous work (Mihelj et al. 2007a), this has been achieved by a mechanical coupling realising a linear displacement of the motor M_1 with the rotation axis a_1 aligned with HH_R. The linear displacement of HH_R depends on θ_1. The resulting distance between HH_{WR} and HH_R is $D_{mean} = 5.1$ mm ($D_{max} = 16.2$ mm) for a subject

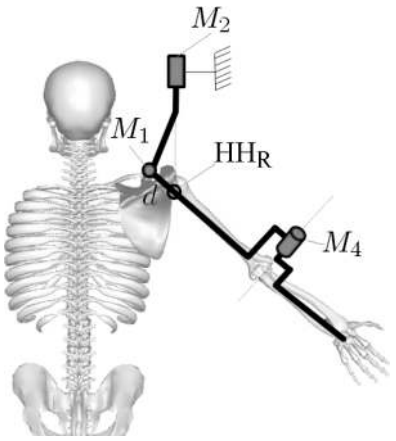

Figure 6. Back view showing a block diagram of the new shoulder actuation principle. Motor M_1 controls the arm elevation angle θ_1, M_2 the angle of the plane of elevation θ_2 and M_4 the elbow angle θ_4. Motor M_3 is not shown. The distance d between motor M_1 and the humerus head HH_R determines the radius of the circle the humerus head travels on.

with body size $h = 170$ cm (Nef and Riener 2008a). Since the coupling mechanics is large and heavy and adds a lot of inertia to the system, an alternative solution is preferred.

One alternative is to select a circular movement to approximate the natural motion of the HH. The basic idea is to approximate the trajectory of HH_{WR} (Figure 5) by a circle with radius d and centre $(M_{1_x}, M_{1_y})^T$ (Figure 6). It is not necessary to take the whole trajectory into account because the ROM of the arm elevation movement is limited to $-45^\circ \leq \theta_1 \leq 135^\circ$. Therefore, the trajectory of HH_R is

$$\begin{pmatrix} x_{HH_R} \\ y_{HH_R} \end{pmatrix} = \begin{pmatrix} M_{1_x} - d\cos(\theta_1 - 90^\circ) \\ M_{1_y} + d\sin(\theta_1 - 90^\circ) \end{pmatrix}. \tag{12}$$

The arising optimisation problem is to find the centre of the circle $(M_{1_x}, M_{1_y})^T$ and the corresponding radius d that minimises D_{mean}. A numerical search within the following limits and step sizes is carried out

$$\begin{aligned} -180\text{ mm} \leq M_{1_x} \leq -120\text{ mm},\ \text{step size}: 1^\circ \\ 50\text{ mm} \leq M_{1_y} \leq 70\text{ mm},\ \text{step size}: 1^\circ \\ 20\text{ mm} \leq d \leq 80\text{ mm},\ \text{step size}: 1^\circ \\ 45^\circ \leq \theta_1 \leq 135^\circ \end{aligned} \tag{13}$$

The result of this search is valid only for patients with body size 1.7 m, but based on Equation (3), the value for other body sizes can be derived by the introduction of a linear scaling factor

$$d_h = d_{h_{ref}} \frac{h}{h_{ref}}. \tag{14}$$

Figure 6 shows a mechanical structure that implements the new shoulder actuation principle. Arm elevation is realised by rotation around the rotation axis a_1 of motor M_1. As a_1 is shifted by the offset distance d from HH_R, HH_R will travel on a spherical trajectory by rotating around M_1.

The rotation axis a_2 of M_2 realising rotation of the plane of elevation is positioned in such a way so that it passes through HH_R. The rotation axis a_3 of M_3 realising internal/external shoulder rotation is aligned with the humerus bone and the rotation axis a_4 of elbow actuation M_4 passes right through the centre of rotation of the elbow.

2.4. ARMin III kinematics

Figure 7 shows a rendered solid model of a robot that realises the new shoulder actuation principle. The human is sitting in a wheelchair (not shown) and his affected arm is connected to the robot. The subject is positioned in the robot such that, for an arm elevation angle $\theta_1 = 90^\circ$, the HH is positioned at the intersection of the two laser beams l_1 and l_2. This is achieved by appropriate manoeuvring of the wheelchair and by adjusting the height of the exoskeleton by means of the motorised lifting column. The human arm is connected to the robot via an upper arm cuff and a lower arm cuff (not shown).

M_2 actuates the rotation of the plane of elevation, and its rotation axis a_2 is marked by the laser beam l_2 and passes through HH_R. The output flange of M_2 connects to P_1, which is a passive rotational joint to adjust the angle ϕ and the distance d (Figure 8). During operation, P_1 is fixed with a screw to a given angle ϕ that depends on the patient's body size with

$$\phi = \arcsin\left(\frac{d}{q_3}\right) = \arcsin\left(\frac{1}{q_3} d_{ref} \frac{h_{body}}{h_{ref}}\right). \tag{15}$$

Motor M_1 actuates the arm elevation angle θ_1 and connects to M_3 via the passive linear joint P_2, which adjusts for the upper arm length l_u. This joint is also fixed during operation. M_3 is composed of a curved slider (R-Guide THK, Ltd., Japan) with radius $q_6 = 9.5$ cm, rotating around axis a_3. Rotation axis a_2 and a_3 intersect in HH_R, thus $q_2 = q_5 + q_6$. The two endings of the curved slider are linked to M_4 and P_3, implementing the elbow actuation. The passive rotation joint P_3 is directly coupled to M_4 and improves the mechanical stability. The lower arm module comprises the passive linear joint P_4 that connects to the hand grasp H. P_4 allows for adjustment of the lower arm length l_l and is blocked during robot operation. All the robot segment lengths are represented and named in Figure 8 and the numerical values are given in Table 2.

As shown in Figure 7, the lower arm part of the robot can be replaced with an actuated lower arm module. This module includes two actuated DOFs for lower

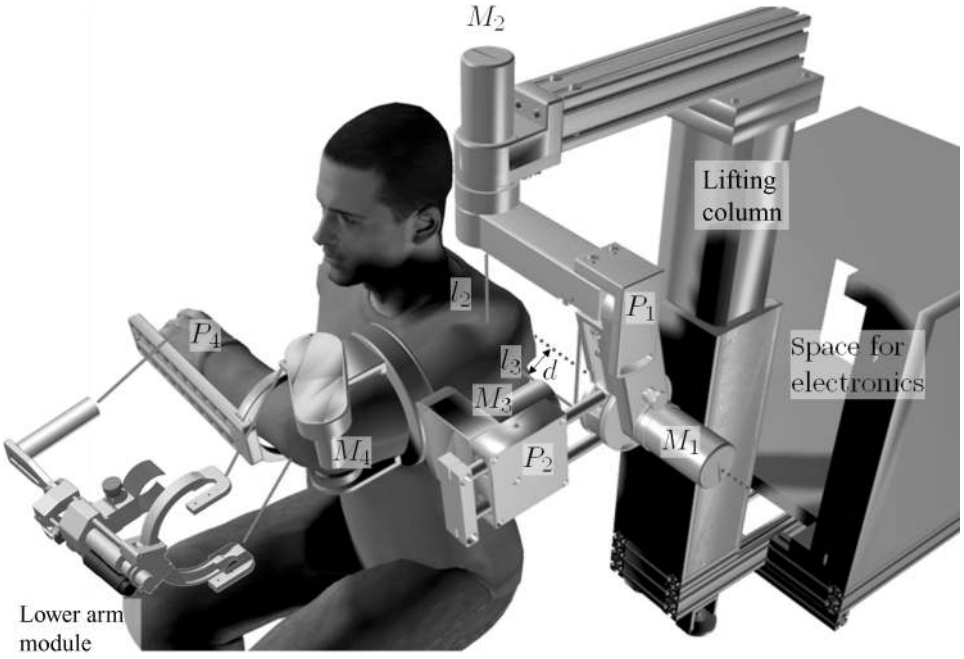

Figure 7. Rendered solid model of the ARMin III robot. The human is sitting in a wheelchair (not shown) in front of the robot. The affected arm is connected to the robotic exoskeleton. The robot has three motors for the shoulder (M_1, M_2, M_3) and one motor for elbow actuation (M_4). The optional lower arm actuation module includes two additional motors for lower arm pro/supination and wrist flexion/extension. The entire exoskeleton is mounted onto an actuated lifting column to adjust for different shoulder heights.

arm pro/supination and wrist flexion/extension. The mass of the actuated lower arm module is $m_5 = 1950$ g.

Figure 7 shows the robot in the configuration for right-arm use. It is possible to switch the device for left-arm use. To do so, the therapist must make sure that no patient is in the device and that the motors are powered off. First, the orientation of the passive joint P_1 must be changed from ϕ to $-\phi$. Then, a 180° counterclockwise rotation around M_2, followed by a clockwise 180° rotation around M_1, brings the robot to the left-arm use configuration. Note that this operation obviously exceeds the ROM of the human arm and, therefore, requires temporary removal of the mechanical safety stops for M_1 and M_2.

2.5. Actuation and identification

2.5.1. Motors

Drives M_1 and M_2 are composed of a Harmonic Drive (HD) gearbox (1:100) directly coupled with the DC motor (Table 3). Drive M_3 is a DC motor that is directly coupled with the HD gearbox (1:30), and the output of the gearbox is coupled to the curved slider via a belt drive (1:14.5). Drive M_4 is a DC motor that is connected to the input of the HD gearbox via a belt drive (1:1), and the output of the HD gearbox (1:100) is coupled to the elbow joint. The belt drive is necessary because, depending on which body side the device is used, the actuator is either above (left-arm use) or below (right-arm use) the elbow joint. The motor could

Table 2. Kinematic data of the ARMin III robot.

	Angle plane of elevation	Arm elevation	Internal/external shoulder rotation	Elbow flexion/extension
Joints	$M_2 : -45° \leq \theta_2 \leq 135°$ $P_1 : -40° \leq \phi \leq +40°$	$M_1 : 45° \leq \theta_1 \leq 135°$ $P_2 : 23.5\text{ cm} \leq l_u \leq 40.5\text{ cm}$	$M_3 : -90° \leq \theta_3 \leq 135°$	$M_4 : 0 \leq \theta_4 \leq 120°$ $P_4 : 10.5\text{ cm} \leq l_l \leq 38.5\text{ cm}$
Segment length	$q_1 = 6.5$ cm $q_2 = 24.5$ cm $q_3 = 22.8$ cm	$q_5 = 15.0$ cm	$q_6 = 9.5$ cm $q_7 = 9$ cm	$q_8 = 6.5$ cm $q_9 = 34$ cm

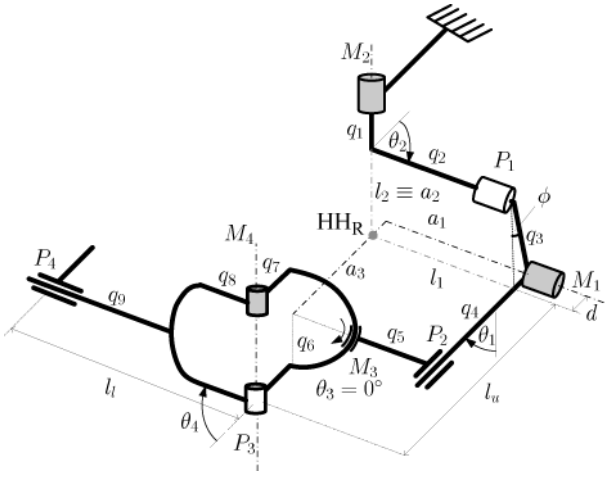

Figure 8. Kinematic chain of the ARMin III robot. The device is actuated by four motors $M_1 - M_4$. Note that the order of rotations is M_2, followed by M_1, M_2 and M_4. The passive joint P_1 allows adjusting the distance d by changing the angle ϕ. Passive joints P_2 and P_4 are linear joints that are used to adjust the upper arm length l_u and the lower arm length l_l. The passive rotatory joint P_3 is directly coupled to motor M_4 and increases mechanical stability of the elbow joint.

therefore not be directly coupled with the HD because it would collide with the human body in the case of right-arm use of the robot.

The joint friction torques have been identified by driving the motors at constant speed while simultaneously measuring the required motor current. The motor torque has been calculated out of the motor current according to $\tau_m = k_s i_m$, with $k_s = 0.052$ mNm/A. A linear function with threshold is used to fit the data. The general form is

$$\tau_{f_j}(\dot{\theta}_j) = \text{sgn}(\dot{\theta}_j)\tau_{s_j} + c_j\dot{\theta}_j \quad (1 \leq j \leq 4). \tag{16}$$

The static friction threshold τ_{s_j} and the parameter c_j describing the coulomb friction were selected by appropriate fitting of the lookup table data. Note that drives M_1 and M_2 are similar and only one of the two need to be identified. Furthermore, it is important to perform the identification in joint positions where gravity does not influence the measurement.

Table 3. Actuation of the ARMin III robot.

Axis	Gear	Motor type
Axis 1: Arm elevation (M_1)	Harmonic Drive[1] 1:100	Maxon Re 35, brushed DC[2]
Axis 2: Angle plane of elevation (M_2)	Harmonic Drive[1] 1:100	Maxon Re 35, brushed DC[2]
Axis 3: Internal/external shoulder rotation (M_3)	Harmonic Drive[1] 1:30 + belt drive 1:14.5	Maxon Re 35, brushed DC[2]
Axis 4: Elbow flexion/ extension (M_4)	Belt Drive 1:1 + Harmonic Drive 1:100	Maxon Re 35, brushed DC[2]

[1] 14 HFUC gearbox, Harmonic Drive Inc., Japan.
[2] Maxon Inc., Switzerland.

The ARMin III robot was demounted to measure the masses m_j of the four moving parts. The centre of gravity and the corresponding radius of gyration r_{cgj} at each part have been determined by finding the point where the part balanced in gravity. The four inertia tensors were determined using a finite element method (FEM) simulation tool that is included in the CAD software (Inventor, Autocad Inc., USA).

2.5.2. Passive weight compensation

For safety reasons, it is required that motor M_1 (arm elevation) be weight-compensated. This is important in order to avoid the robot collapsing in case of power loss. Moreover, the passive weight compensation also significantly reduces the continuous torque that motor M_1 must deliver.

The weight compensation must offset the gravitational torque τ_{g1} acting onto motor M_1. τ_{g1} depends on the elbow angle θ_4. It is maximal for full extended elbow ($\theta_4 = 0°$). In this case, it is

$$\tau_{g1} = (r_{cg1}m_1 + (l_u - q_7 + r_{cg3})m_3 + (l_u + r_{cg4})m_4)g \sin(\theta_1) \quad \text{for } \theta_4 = 0°, \tag{17}$$

with the radius of gyration r_{cgj} measured from the rotation axis of the motor M_j, m_j the mass of the element j, g the constant of gravity and θ_1 the arm elevation angle. Note that the torque varies with the sine of the arm elevation and, therefore, the passive weight support should too.

Figure 9 shows the proposed mechanism with a spring that connects to the output flange of M_1 via a cable. The cable is guided by two pulleys and deviated by two more pulleys at point D. The cable is fixed to the flange at point F. The force exercised by the spring is $F_s = (|\boldsymbol{DF}| + x_0)k_s$, where $|\boldsymbol{DF}|$ is the spring deflection, x_0 is the length offset and k_s is the spring constant. The length of the cable should be selected such that the offset $x_0 = 0$. This is achieved when the cable ends at point D with deflected spring. This is equivalent to claim that

$$F_s = |\boldsymbol{DF}|k_s. \tag{18}$$

If Equation (18) is fulfilled, then the torque that the spring exercises onto M_1 is

$$\tau_{s1}|\boldsymbol{DC}| \cdot |\boldsymbol{CF}|k_s \sin(\theta_1), \tag{19}$$

with $|\boldsymbol{DC}| = 101$ mm and $|CF = 56$ mm$|$ the distance between the deviation point D and the centre C, i.e. the distance between the centre C and the cable fixation point

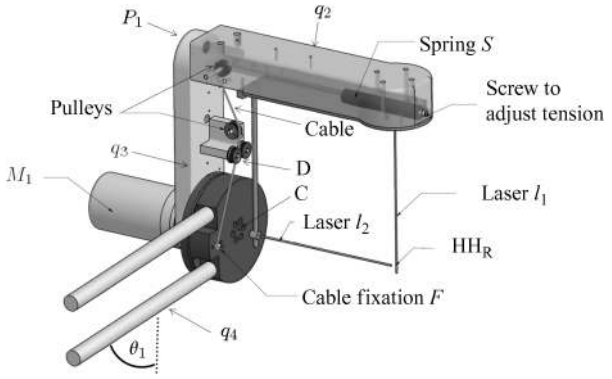

Figure 9. Spring mechanism for passive weight compensation. The mechanism allows a 180° counterclockwise rotation of q_4 around M_1. This is required for left-arm/right-arm use changes.

F and the spring constant k_s. As the spring torque τ_{s1} should be equal to τ_{g1}, the following equation determines the selection of the spring:

$$k_s = \frac{(r_{cg1}m_1 + (l_u - q_7 + r_{cg3})m_3 + (l_u + r_{cg4})m_4)g}{|DC| \cdot |CF|}. \tag{20}$$

The maximal spring deflection occurs at $\theta_1 = 0°$ and is $s_{max} = |DC| + |CF| - x_0 = 157$ mm for $x_0 = 0$ mm. This position is outside the ROM of M_1 and is never reached during normal operation. However, when the robot is switched from right- to left-side use, this position is reached. Therefore, the spring parameters need to be carefully selected in order to not overpass the maximal spring deflection.

2.6. *Sensors and control hardware*

All DC motors are equipped with optical incremental encoder (1000 count/rotation) and wire potentiometers for redundant position measurement. The controller runs on a Matlab/Simulink XPC target (The MathWorks, Inc., USA) computer with a loop time of 1 ms. Analogue channels provide output for the current amplifiers (Maxon 4-Q-DC servoamplifier ADS 50/50; Maxon AG, Switzerland). The encoder signals and the analogue signals from the redundant potentiometer position sensors are interfaced to the multiple input/output interface card (Measurement & Computing, Inc., USA).

The graphical user interface runs on a computer with the Windows operating system (Microsoft Corporation, USA) and is connected with the real-time target by a local area network using TCP/IP protocol.

2.7. *Passive and active safety*

Passive safety features (no sharp edges, skin biocompatible cuffs, mechanical end stops to guarantee that no joint can exceed the anatomical ROM, etc.) are combined with active safety features. Four redundant absolute position-sensing potentiometers, one for each joint, allow detecting malfunction of a digital encoder. The real-time controller (XPC Target) is supervised by a hard-coded watchdog that interrupts motor power in case of absence of the 100 Hz service pulses. Several surveillance routines are implemented in the software. These include current and speed monitoring and a collision detection algorithm.

Whenever an abnormal event is detected, the safety circuit immediately cuts the power of the motor drives. As the robot is equipped with a passive weight compensation system for motor M_1, it does not collapse after power loss. The motor M_3 does not have passive weight compensation, but the relatively high friction keeps the joint in position in case of power loss. This is not the case for motor M_4 where in some positions it can happen that the elbow moves into full flexion in case of power loss. Since the moving mass m_4 of the elbow joint is small and close to the centre of rotation, and because of the joint friction, this movement is not fast and it stops at the mechanical end stop. The drive M_1 is not affected by gravity. Since all drives are backdrivable, the robot can easily be moved manually by a therapist in order to release the patient from a potentially uncomfortable posture.

Last but not least, at this stage, a physiotherapist always observes the training holding a deadman switch in his hand. Releasing the switch interrupts the motor power and stops the robot immediately. This can also be achieved by pressing the emergency stop button. It is expected that future robots will not require permanent supervision and that the deadman switch could be omitted.

Besides patient safety, the safety of the therapist needs to be considered too. As the robot does not know the position of the therapist, it is important that the therapist is aware of the danger of collisions with the robot. Nevertheless, the probability of a severe accident is low because of the fact that the maximal speed of the robot is limited by surveillance circuits. A detailed risk analysis, as required from the legal bodies, shows that the risk for a patient and a therapist using the robot is acceptable with respect to the expected rehabilitation benefit for the patient. Consequently, the ethics committee has authorised the use of the ARMin III robot with both patients and healthy subjects (Zurich, Switzerland).

3. Results

3.1. *Human shoulder*

Equations (8)–(10) describe the motion of the humerus, the scapula and the clavicle during arm elevation. This data has been used to animate segmented CT data to visualise the motion of the human shoulder. Figure 10 shows screenshots of shoulder postures for distinct arm elevation angles.

The screenshots show that in the first phase of the arm elevation movement, starting at $\theta_1 = 0°$ and ending at

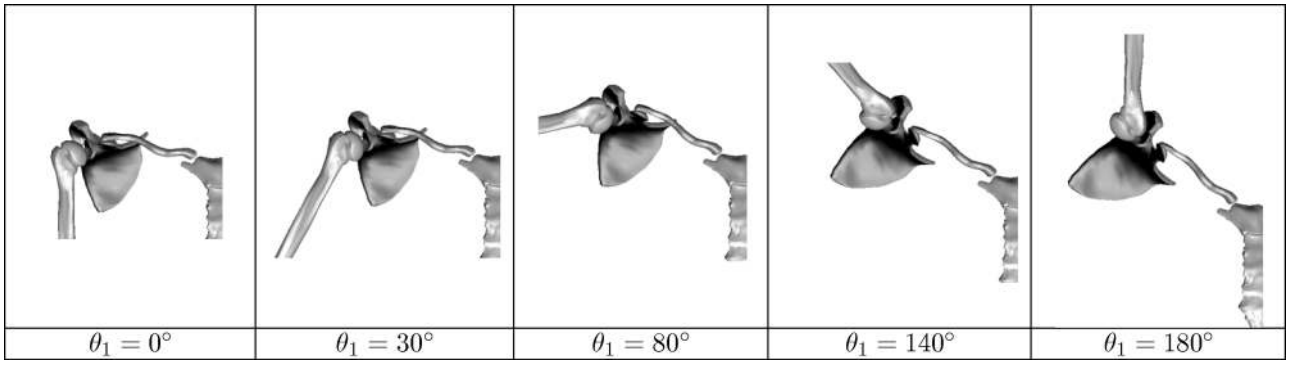

Figure 10. Human shoulder postures during an unrestricted arm elevation movement without robotic device.

$\theta_1 = 80°$, the rotation happens mainly in the glenohumeral joint. At $\theta_1 = 80°$, the scapula starts to tilt, and during the phase $80° \leq \theta_1 \leq 140°$, the scapula tilting movement is predominant. The last phase, bringing the arm up to 180°, is again characterised by predominant glenohumeral rotation.

3.2. The robotic shoulder

The natural motion of the HH has been replaced by a circular motion. The parameters of this circular motion, i.e. centre of rotation and radius, were determined by a numerical optimisation with the goal to find the best fit between unrestricted natural and robotic motions. According to Equation (11), the centre of rotation and the radius that minimise the distance D_{mean} have been determined as

$$\begin{aligned} (M_{1_x}, M_{1_y})^{\mathrm{T}} &= (-158 \text{ mm}, 53 \text{ mm})^{\mathrm{T}} \quad D_{\text{mean}} = 2.8 \text{ mm} \\ d &= 36 \text{ mm} \qquad\qquad\qquad\quad D_{\text{max}} = 10.9 \text{ mm} \\ \text{for} \quad 45° &\leq \theta_1 \leq 135° \end{aligned} \tag{21}$$

These values are valid for a person with body size $h = 1.7$ m. Equations (14) and (15) are used to calculate the values d and the tilting angle ϕ for subjects of different body sizes. These values and the corresponding values for D_{mean} and D_{max} are presented in Table 4.

3.3. Mechanics

Five ARMin III robots have been built and are now being used for clinical investigations.

Figure 11 shows the robot with a healthy subject sitting in a wheelchair with the right arm connected to the robot. A graphical display presents different therapeutic tasks. These tasks include scenarios to train eating and drinking, ball game scenarios, ping-pong scenarios, labyrinth scenarios and others (Nef et al. 2007a, 2007b). Loudspeakers are used to increase the level of realism of the training.

The device can be easily switched from right-arm to left-arm use. The intersection point of two laser pointers mark the desired position of the HH for an arm elevation angle $\theta_1 = 45°$, which helps the therapist to position the patient. The upper arm length of the robot can be adjusted by turning a small handle located at the end of the two aluminium cylinders (link q_4). The lower arm length is adjusted by moving the handle along a linear rail (link q_9). As shown in Figure 7, it is possible to connect a lower arm actuation module to the ARMin III device. It is a reinforced version of the lower arm actuation module that has been used with the ARMin II device (Mihelj et al. 2007a) and it has two motors to actuate lower arm pro/supination and wrist flexion/extension.

The maximal torque $\tau_{g1} = 27.88$ Nm acting on M_1 due to gravity has been calculated with Equation (17) for upper arm length $l_u = 30$ cm. Optimal compensation with zero offset and fulfillment of Equation (18) is achieved with the spring constant $k'_s = 4929$ N/m (20). Since the choice of springs is limited, a spring constant of $k_s = 10,185$ N/m has been selected. The deflected spring length is $l_0 = 105$ mm, diameter $D = 36.5$ mm, wire diameter $D_w = 5$ mm, wire material stainless steel 1.1200C and

Table 4. Shoulder actuation parameters for patients with different body sizes h.

h [cm]	150	155	160	165	170	175	180	185	190	195	200	205	210
d [mm]	31.76	32.82	33.88	34.94	36.00	37.06	38.12	39.18	40.24	41.29	42.35	43.41	44.47
ϕ [°]	7.06	7.54	8.04	8.56	9.09	9.63	10.20	10.78	11.38	11.99	12.63	13.28	13.94
D_{mean} [mm]	2.47	2.55	2.64	2.72	2.80	2.88	2.96	3.05	3.13	3.21	3.29	3.38	3.46
D_{max} [mm]	9.62	9.94	10.26	10.58	10.90	11.22	11.54	11.86	12.18	12.50	12.82	13.14	13.46

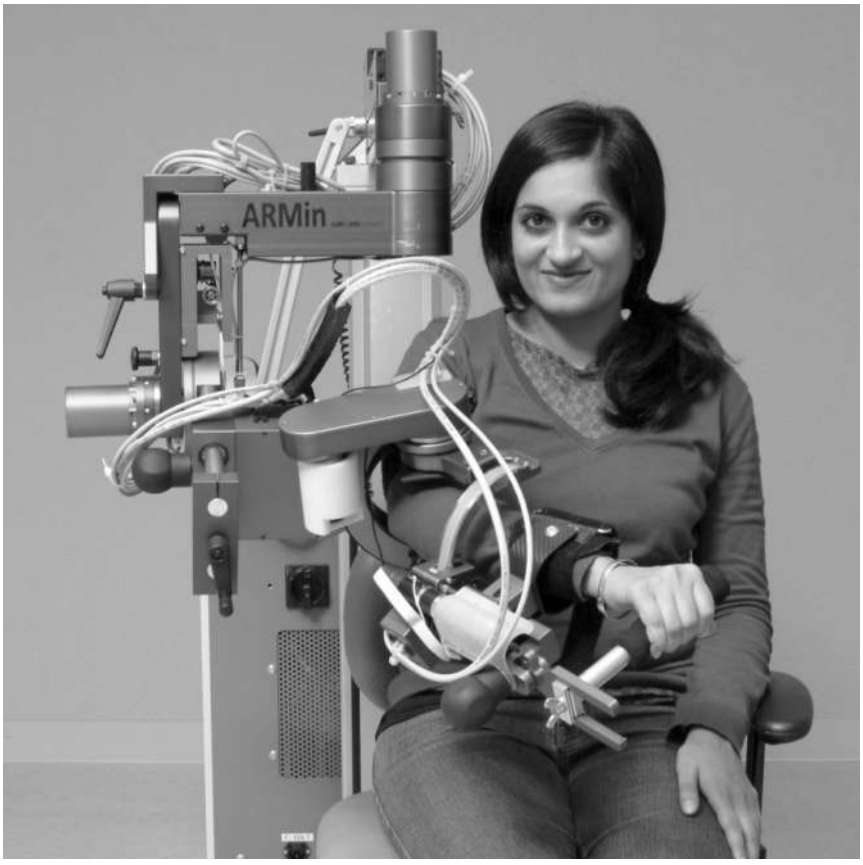

Figure 11. ARMin III robot with a healthy subject. The lower arm actuation module with two motors for lower arm pro/supination and wrist flexion/extension is shown too. The ARMin III exoskeleton connects to the hand, the forearm and the upper arm. At the hand, there is not really an attachment, but the hand grasps a cylindrical bar. Two adjustable and replaceable cuffs (Nef et al. 2007a) accommodate forearm and upper arm. The exoskeleton is symmetric and can be used for both arms.

maximal repetitive deflection $s_n = 83.86$ mm. The spring has been mounted with a cable offset $x_0 = 0.065$ m to compensate for the difference between the spring constants. Due to the spring offset, Equation (18) is no longer fulfilled, and the resulting equilibrium point is at $\theta_1 = 77^\circ$. Maximal spring deflection and maximal spring force occur at $\theta_1 = 0^\circ$ and are $s_{\max} = |DC| + |itCF| - x_0 = 92$ mm and $F_{s_{\max}} = 937$ N.

The technical specifications of the ARMin III device are presented in Table 5. All values are measured on the robot and all values are worst-case values. For example, the measurement of the maximal acceleration $\ddot{\theta}_{4_{\max}}$ has been carried out in the position with the highest influence of gravity ($\theta_1 = 90^\circ, \theta_3 = 90^\circ, \theta_4 = 0^\circ$).

4. Discussion

4.1. Shoulder actuation

A quantitative description of the glenohumeral motion in healthy subjects of different body sizes has been developed. The model is very much simplified. It does not take into account the angle of the plane of elevation θ_2. Figure 1 shows the vertical translation of the HH during arm elevation. A similar picture could be presented for the horizontal motion of the humerus during horizontal ante-retro-version of the arm (Schiele and van der Helm 2006). This simplification might lead to model errors and could be improved. Furthermore, the assumption that additional external mass does not affect the position of the scapula nor the position of the HH is obviously not fully true (Kon et al. 2008). The movement of the HH will also differ among individuals (Kon et al. 2008) and it might also depend on age (Karduna et al. 2001) and also on the level of neurological injury (Niessen et al. 2008).

The advantage of the proposed model is that it is simple enough to be realised in an exoskeleton robot. Besides its shortcomings, it represents the principal relation between the arm elevation angle and the vertical position of the HH. It is not perfect, but a mechanism that implements this model will result in a more ergonomic shoulder actuation than a ball-and-socket-joint-type shoulder actuation.

The ARMin III robot provides *vertical* translation movement of the HH, with a simple mechanical structure.

Table 5. Technical data of the ARMin III device.

Maximal end-point load[a,c]	4.6 kg
Weight (excluding controller, hardware, frame)[c]	18.755 kg
Repeatability (endpoint)[c]	±0.5 mm
Stiffness (endpoint)[a,d]	0.364 mm/N
Force (endpoints)[a,c]	$F_{\max} = (451\text{ N}, 804\text{ N}, 706\text{ N})^{\mathrm{T}}$ with $G = (-g, 0, 0)^{\mathrm{T}}$
Bandwidth for small end-point movements (±1.5 cm)[b]	1.28 Hz

	Axis 1 – Arm elevation	Axis 2 – Plane of elevation	Axis 3 – Internal/external shoulder rotation	Axis 4: Elbow flexion/extension
ROM: $\theta_{j\min}, \theta^{b}_{j\max}$	$46^\circ \le \theta_1 \le 140^\circ$	$-47^\circ \le \theta_2 \le 135^\circ$	$-91^\circ \le \theta_3 \le 92^\circ$	$0^\circ \le \theta_1 \le 123^\circ$
Static friction threshold $\tau^{c,e}_{\mathrm{s}_j}$	5.17 ± 0.17 mNm	5.17 ± 0.17 mNm	17.45 ± 0.89 mNm	7.16 ± 0.22 mNm
Coulomb friction parameter $c^{c,e}_j$	0.0365 mNms/°	0.0365 mNms/°	0.159 mNms/°	0.1453 mNms/°
Breakaway torque user-driven motions[f]	0.95 Nm	0.95 Nm	5.9 Nm	1.2 Nm
Maximal velocity: $\dot{\theta}^{c}_{j\max}$	176°/s	178°/s	102°/s	163°/s
Maximal acceleration: $\ddot{\theta}^{c,h}_{j\max}$	357°/s²	741°/s²	7222°/s²	8750°/s²
Maximal torque: $\tau^{c,h}_{j\max}$	37.76 Nm	33.28 Nm	≫ 38.5 Nm	32.0 Nm
Bandwidth for small movements, measured with $\theta_{\mathrm{ref}_j} = 2^\circ \sin(2\pi f)$[b]	1.68 Hz	1.4 Hz	2.2 Hz	1.8 Hz
Moving mass: m_j	$m_1 = m_{1\mathrm{a}} + m_{1\mathrm{b}}$ 2.28 kg + 3.49 kg	$m_2 = 7.060$ kg	$m_3 = 3.610$ kg	$m_4 = 2.315$ kg
Radius of centre of gravity: r^{g}_{cg}	$r_{\mathrm{cg1}} = 0.6(l_{\mathrm{u}} - d) - 0.02$ m	$r_{\mathrm{cg2}} = 0.195$ m	$r_{\mathrm{cg3}} = 0.02$ m	$r_{\mathrm{cg4}} = 0.17$ m

Note. All data is measured on the device.
[a] Worst case exoskeleton position.
[b] Measured with healthy subject.
[c] Measured without subject (exoskeleton only).
[d] Stiffness measured at the endpoint by applying 20 N, while the motors are position controlled.
[e] According to Equation (24), the overall friction torque is $\tau_{\mathrm{f}_j}(\dot{\theta}_j) = \mathrm{sgn}(\dot{\theta}_j)\tau_{\mathrm{s}_j} + c_j\dot{\theta}_j \quad (1 \le j \le 4)$.
[f] An additional force sensor (6 DOF, JR3 Inc., USA) has been used to measure the breakaway torques. Details can be found in Nef et al. (2008b).
[g] r_{cg1} varies with the adjustable upper arm length l_{u} and with the distance d. It is $r_{\mathrm{cg1}} = \frac{1}{m}(r_{1\mathrm{a}}m_{1\mathrm{a}} + r_{1\mathrm{b}}m_{1\mathrm{b}}) = \frac{1}{5.77\,\mathrm{kg}}(0.105\,\mathrm{m} \times 2.28\,\mathrm{kg}) + (l_{\mathrm{u}} - d - q_7 - 0.01\,\mathrm{m})3.49\,\mathrm{kg})$. r_{cg4} varies with the lower arm length l_{l}, but as the handle is lightweight, the variations are very small and therefore neglected.
[h] The motor current of axis 3 is limited to 3 A. The current for the other axis is limited to 10 A.

The device can be changed from left- to right-side use without requiring any tool, and within less than 1 min. Laser pointers mark the desired position of the HH and make the patient positioning easier.

Compared to the kinematics of the MGA-Exoskeleton (Carignan and Liszka 2005), where circular motion of the HH is realised via an additional motor that lifts up the exoskeleton, the presented device is cheaper and safer because of the implementation of circular motion without additional actuation. One disadvantage of the ARMin III robot is that vertical translation of the HH is possible only when it is accompanied by an arm elevation movement. This allows the training of ADL movements, but not the training of specific shoulder movements (e.g. in vertical translational direction) as they can be trained with the MGA-Exoskeleton.

The vertical translation movement of the HH seems to be important for movements with large ROM only. As long as the arm elevation angle θ_1 is below $80^\circ - 90^\circ$, the vertical translation is small, and therefore ball-and-socket-type shoulder actuation could be used. Since many ADL movements require moving the arm above the head (Nef et al. 2007a), this feature has been implemented in the ARMin III design. However, it needs to be investigated as to what percentage of the intended patients will be able to use to full ROM.

The ARMin III robot does not provide *horizontal* translation movement of the HH. This might lead to misalignment between the robot and the HH. Nevertheless, it has been observed that the misalignments resulting from horizontal translation of the HH are smaller than the ones resulting from vertical translation. Furthermore, the patients tend to compensate for horizontal motion of the HH by doing small translational movements of the trunk. The passive Armeo device (Sanchez et al. 2006) uses one additional passive rotational joint to follow horizontal displacement of the HH. This approach works well in passive devices with low inertia and, in a modified and extended form, is also used in the passive Dampace exoskeleton (Stienen et al.

2007). It is anticipated that this approach would not work for the actuated ARMin III robot because of the higher inertia. In the current ARMin III device, reaction torques and forces, as they occur when the robot exercises torques onto the human arm, i.e. during acceleration/deceleration, are transferred via the frame to the ground. If one would add a passive joint between the ARMin III exoskeleton and the frame, then part of the reaction torques could no longer be transferred to the frame and would be applied to the human shoulder. This is not ergonomic and is expected to feel uncomfortable. One valid approach could be to add a mechanically coupled rotational DOF between the ARMin III exoskeleton and the frame. The joint would be coupled to the drive M_2 that actuates the plane of elevation. Nevertheless, since this has never been an issue during the extensive use of the ARMin II robot (Nef et al. 2007a), it is unlikely that this passive will be added to the ARMin III robot.

One critical factor of the ARMin shoulder actuation is that lateral displacement of the human arm in the exoskeleton might influence the trajectory of the HH. Such displacement could happen during arm elevation if the cuffs are loose and if the elbow is fully extended.

4.2. Mechanics and actuation

The weight of the ARMin III exoskeleton (excluding controller, hardware, frame) is 18.755 kg. Compared to other exoskeletons this is rather heavy. For example, the weight of the MGA-Exoskeleton is 12 kg (Carignan and Liszka 2005) while the weight of Rosen's exoskeleton is 6.8 kg only (Perry and Rosen 2006). Since the ARMin III exoskeleton is not intended to be wearable, this is acceptable. Furthermore, the links must be strong enough to allow the required 3-kg end-point load. One disadvantage is that for fast, user-driven movements, the user will feel the inertia of the system. Computed torque or disturbance compensation in general cannot be applied here, since for an operator-guided haptic interface like ARMin, motions are not known beforehand. The operator is free to move in arbitrary ways. ARMin has no acceleration sensors, only position sensors. Without acceleration sensors, the forces caused by inertia are not known early enough. Inertial forces cannot be given as a function of time or of the states, as needed for compensation. It can be shown theoretically that double differentiation of the position to obtain acceleration for inertia compensation will lead to unstable behaviour of the robot because of the phase delay (Colgate 1988). Compensation of inertia would be possible using force feedback, but the robot does not use force sensors. Thus, with the current system, there is no way to reduce inertial effects. The exoskeleton is currently made out of aluminium. Therefore, the weight could be reduced by using carbon fibre composites, as is suggested by others (Sugar et al. 2007). Since the ARMin device is exclusively designed for rehabilitation applications with rather slow movements, it is unlikely that future work will be dedicated to reduce the weight of the device.

The ROM of the exoskeleton meets the ROM of the human arm, except for the arm elevation movement, where the ROM of the robot is limited by mechanical end stops to $46^\circ \leq \theta_1 \leq 140^\circ$ for safety reasons.

The passive weight compensation of the arm elevation movement is a key element of the exoskeleton and it works satisfactorily. It has been observed that the actual compensation torque becomes smaller with wear. Therefore, periodic readjustment of the spring tension is required. One reason for that effect could be that the maximal repetitive deflection $s_n = 83.86$ mm of the spring is exceeded by 10.5% when the device is switched from right-side use to left-side use and vice versa. The current spring is made of stainless steel 1.1200C. Replacing this spring by a spring made of another alloy with a higher repetitive deflection should be considered. Furthermore, it would be nice to select a spring that fits with zero offset cable length and fulfills Equation (18). Note that due to the offset, and due to the influence of the elbow angle θ_4, the spring compensation torque does not always correspond to the gravitational torque and the difference between the two must be compensated for by the drive M_1. The mean value of the difference that the motor M_1 must compensate for is 3.46 Nm. It has been observed that the pulleys for the cable deviation (Figure 9) are critical components and must be carefully selected. In a first attempt, pulleys with sliding contact bearing have been used. However, the friction in the pulleys was too high, the pulleys did not properly roll and rubbing between the pulleys and the cable occurred. As a consequence, the cable broke after 30 hrs of intensive use. Therefore, it is important to use high-quality pulleys with ball bearings.

The measured breakaway torques, i.e. the amount of torque that the user must produce to overcome static joint friction to initiate a user-driven movement, are small ($\leq$1.2 Nm) for drives 1, 2 and 4. Friction in drive 3 is higher, and the breakaway torque is 5.9 Nm. The friction for the internal/external shoulder rotation is a trade-off between safety and performance of the open-loop impedance controller. On the one hand, the robot's joint falling down in case of power loss must be avoided, and on the other hand, it is important that the user can easily initiate a movement. The first version of the ARMin device had a custom-made low-friction cable-driven actuator for the internal/external shoulder rotation and the performance of the impendence controller was excellent. But for safety reasons, the joint was often fixed in one position (Nef et al. 2007a). Therefore, recent work has been dedicated to develop a new open-loop impedance controller that compensates for both static and dynamic friction (Nef and Lum 2009).

The measured velocities, accelerations and torques (Table 5) are in the range of the specified values (Table 1) and are sufficient for rehabilitation purposes. The only limitation is that the maximal velocity of the internal/external shoulder rotation is $\dot{\theta}_{3_{\max}} = 102^\circ/\text{s}$ instead of the required $150^\circ/\text{s}$. The internal/external shoulder rotation is driven by a DC motor, followed by an HD gearbox (1:30) and a belt

drive (1:14.5) (Table 3). Since both the torque and the acceleration are higher than required, it would be obvious to use an HD gearbox with a smaller reduction ratio. Unfortunately this is not available. To fix the problem one could replace the HD with a planetary gear with a 1:15 reduction ratio. Precautions must be taken to be certain that the resulting friction force is high enough to make sure that the arm does not fall down in the case of power loss (cf. Section 2.7).

5. Conclusion

The ARMin III device as described in this paper is an exoskeleton that has been optimised for clinical use as rehabilitation robot. It provides 3 DOF for the shoulder, 1 DOF for the elbow and 2 optional DOF for lower arm pro/supination and wrist flexion/extension. Novelty and key benefits of the device are the new shoulder actuation principle and the fact that the device can easily be used for left and right arms. The mechanics of the new shoulder actuation is simple and only slightly more complex than the ball-and-socket-joint-type shoulder actuations. For clinical use, left/right side changes are crucial for an economic use of the device.

Five ARMin III devices have recently been installed in hospitals in Switzerland (Balgrist University Hospital, Rehabilitation Hospital Rheinfelden, Zurich University Hospital) and in the United States (National Rehabilitation Hospital, Washington, DC). The devices are currently tested on chronic stroke subjects. Future work will be conducted for clinical evaluation, development of a hand module for grasping tasks, and development of new patient-cooperative control strategies.

Acknowledgements

This work was supported in part by the ETH Foundation, the Swiss Research Foundation NCCR on Neural Plasticity and Repair, the Gottfried and Julia Bangerter-Rhyner Foundation, a Fellowship from the National Science Foundation and the Hans-Eggenberger Foundation. We thank Andreas Brunschweiler and Alessandro Rotta from the ETH Zurich and the occupational therapists and Prof. Dr. V. Dietz of the Balgrist University Hospital, Zurich, for their contributions to this work. Furthermore, we thank Dr. Gery Colombo from Hocoma AG, Volketswil, Switzerland, for his contributions.

References

Bagg SD, Forrest WJ. 1988. A biomechanical analysis of scapula rotation during arm abduction in the scapula plane. Am J Phys Med Rehabil. 67(6):238–245.

Bayona NA, Bitensky J, Salter K, Teasell R. 2005. The role of task-specific training in rehabilitation therapies. Top Stroke Rehabil. 12:58–65.

Bergamasco M, Borelli L, Carboncini MC, Frisoli A, Marcheschi S, Montagner A, Procopio C, Rossi B, Sals1edo F, Tolaini M. 2007. Arm rehabilitation with a robotic exoskeleleton in Virtual Reality. Proceedings of the IEEE 10th International Conference on Rehabilitation Robotics; June 13–15; Noordwijk, The Netherlands, pp. 631–642.

Brainin M, Bornstein N, Boysen G, Demarin V. 2000. Acute neurological stroke care in Europe: results of the European stroke care inventory. Eur J Neurol. 7:5–10.

Butefisch C, Hummelsheim H, Denzler P, Mauritz KH. 1995. Repetitive training of isolated movements improves the outcome of motor rehabilitation of the centrally paretic hand. J Neurol Sci. 130:59–68.

Carignan C, Liszka M. 2005. Design of an arm exoskeleton with scapula motion for shoulder rehabilitation. Proceedings of the 12th International Conference on Advanced Robotics; July 18–20; Seattle, USA, pp. 524–531.

Cheng JC, Leung SS, Chiu BS, Tse PW, Lee CW, Chan AK, Xia G, Leung AK, Xu YY. 1998. Can we predict body height from segmental bone length measurements? A study of 3,647 children. J Pediatr Orthop. 18(3):387–393.

Colgate JE. 1988. The control of dynamically interacting systems. Massachusetts Institute of Technology, Department of Mechanical Engineering.

Coote S, Stokes E, Murphy B, Harwin W. 2003. The effect of GENTLE/s robot-mediated therapy on upper extremity dysfunction post stroke. Proceedings of the 8th International Conference on Rehabilitation Robotics; April 23–25; Daejeon, Korea, pp. 59–61.

Culham E, Peat M. 1993. Functional anatomy the shoulder complex. J Orthop Sports Phys Ther. 18(1):342–350.

De Groot JH, van Woensel W, van der Helm FCT. 1999. Effect of different arm loads on the position of the scapula in abduction postures. Clin Biomech. 14(5):309–314.

Dewald J, Ellis MD, Holubar BG, Sukal T, Acosta AM. (2004). The robot application in the rehabilitation of stroke patients. Neurol Rehabil. (4):S7.

Doody SG, Freedman L, Waterland CJ. 1970. Shoulder movements during abduction in the scapular plane. Arch Phys Med Rehabil. 51(10):595–604.

Fanin C, Gallina P, Rossi A, Zanatta U, Masiero S. 2003. NeReBot: a wire-based robot for neurorehabilitation. Proceedings of the 8th International Conference on Rehabilitation Robotics; April 23–25; Daejeon, Korea, pp. 23–26.

Freedmann L, Munro RR. 1966. Adduction of the arm in the scapular plane: scapular and glenohumeral movements: a roentgenographic study. J Bone Joint Surg Am. 48:1503–1510.

Hesse S, Werner C, Pohl M, Rueckriem S, Mehrholz J, Lingau ML. 2005. Computerized arm training improves the motor control of the severely affected arm after stroke. Stroke. 36:1960–1966.

Hogan N. 1984. An organizing principle for a class of voluntary movements. J Neurosci. 4:2745–2754.

Kahn LE, Lum PS, Rymer WZ, Reinkensmeyer DJ. 2006. Robot-assisted movement training for the stroke-impaired arm: Does it matter what the robot does? J Rehabil Res Dev. 43(5):619–630.

Karduna AR, McClure PW, Michener LA, Sennett B. 2001. Dynamic measurements of three-dimensional scapular kinematics: a validation study. J Biomech Eng. 123(2):184–190.

Kon Y, Nishinaka N, Gamada K, Tsutsui H, Banks SA. 2008. The influence of handheld weight on the scapulohumeral rhythm. J Shoulder Elbow Surg. 17(6):943–946.

Krebs HI, Ferraro M, Buerger SP, Newbery MJ, Makiyama A, Sandmann M, Lynch D, Volpe BT, Hogan N. 2004. Rehabilitation robotics: pilot trial of a spatial extension for MIT-Manus. J Neuroeng Rehabil. 1:5.

Kwakkel G, Kollen BJ, Krebs HI. 2008. Effects of robot-assisted therapy on upper limb recovery after stroke: a systematic review. Neurorehabil Neural Repair 22(2):111–121.

Kwakkel G, Wagenaar RC, Twisk JWE, Langkhorst GJ, Koetsier JC. 1999. Intensity of leg and arm training after primary middle-cerebral artery stroke: a randomized trial. Lancet 35:191–196.

Lenarcic J, Stanisic M. 2003. A humanoid shoulder complex and the humeral pointing kinematics. IEEE Trans Robot Autom. 19(3):499–506.

Lum PS, Burgar CG, Shor PC. 2004. Evidence for improved muscle activation patterns after retraining of reaching movements with the MIME robotic system in subjects with post-stroke hemiparesis. IEEE Trans Neural Syst Rehabil Eng. 12(2):186–94.

Mihelj M, Nef T, Riener R. 2007a. ARMin II – 7 DoF rehabilitation robot: mechanics and kinematics. Proceedings of the IEEE international conference on Robotics and Automation; April 10–14; Rome, Italy, pp. 4120–4125.

Mihelj M, Nef T, Riener R. 2007b. A novel paradigm for patient-cooperative control of upper limb rehabilitation robots. Adv Robot. 21(8):843–867.

Moeslund TB, Madsen CB, Granum E. 2005. Modelling the 3D pose of a human arm and the shoulder complex utilizing only two parameters. J Integr Comput Aided Eng. 12(2):159–175.

Nef T, Lum P. 2009. Improving backdrivability in geared rehabilitation robots. Med Biol Eng Comput. 2009 Jan 30. [Epub ahead of print]

Nef T, Mihelj M, Kiefer G, Perndl C, Muller R, Riener R. 2007b. ARMin – exoskeleton for arm therapy in stroke patients. Proceedings of the IEEE 10th International Conference on Rehabilitation Robotics; June 13–15; Noordwijk, The Netherlands, pp. 68–74.

Nef T, Mihelj M, Riener R. 2007a. ARMin: a robot for patient-cooperative arm therapy. Med Biol Eng Comput. 45:887–900.

Nef T, Riener R. 2008. Shoulder actuation mechanisms for arm rehabilitation exoskeletons. Proceedings of the second IEEE/RAS-EMBS International Conference on Biomedical Robotics and Biomechanics; October 19–22; Scottsdale, AZ, USA.

Niessen M, Janssen T, Meskers C, Koppe P, Konijnenbelt M, Veeger D. 2008. Kinematics of the contralateral and ipsilateral shoulder: a possible relationship with post-stroke shoulder pain. J Rehabil Med. 40(6):482–486.

Oldewurtel F, Mihelj M, Nef T, Riener R. 2007. Patient-cooperative control strategies for coordinated functional arm movements. Proceedings of the European Control Conference; July 2–5, Kos, Greece.

Perry JC, Rosen J. 2006. Design of a 7 degree-of-freedom upper-limb powered exoskeleton. Proceedings of the first IEEE/RAS-EMBS International Conference on Biomedical Robotics and Biomechanics; February 20–22; Pisa, Italy.

Platz T. 2003. Evidenzbasierte armrehabilitation: Eine systematische literaturübersicht. Nervenarzt 74:841–849.

Prange GB, Jannink MJ, Groothuis-Oudshoorn CG, Hermens HJ, Ijzerman MJ. 2006. Systematic review of the effect of robot-aided therapy on recovery of the hemiparetic arm after stroke. J Rehabil Res Dev. 43(2):171–184.

Reinkensmeyer DJ, Kahn LE, Averbuch M, McKenna-Cole A, Schmit BD, Rymer WZ. 2000. Understanding and treating arm movement impairment after chronic brain injury: progress with the ARM guide. J Rehabil Res Dev. 37(6):653–662.

Riener R, Fuhr T. 1998. Patient-driven control of FES-supported standing-up: A simulation study. IEEE Trans Rehabil Eng. 6:113–124.

Riener R, Lünenburger L, Jezernik S, Anderschitz M, Colombo G, Dietz V. 2005a. Cooperative subject-centered strategies for robot-aided treadmill training: first experimental results. IEEE Trans Neural Syst Rehabil Eng. 13:380–393.

Riener R, Nef T, Colombo G. 2005b. Robot-aided neurorehabilitation for the upper extremities. Med Biol Eng Comput. 43:2–10.

Rosamond W, Flegal K, Friday G, Furie K, Go A, Greenlund K, Haase N, Ho M, Howard V, Kissela B, Kittner S, Lloyd-Jones D, McDermott M, Meigs J, Moy C, Nichol G, O'Donnell CJ, Roger V, Rumsfeld J, Sorlie P, Steinberger J, Thom T, Wasserthiel-Smoller S, Hong Y; American Heart Association Statistics Committee and Stroke Statistics Subcommittee. 2007. Heart disease and stroke statistics–2007 update: a report from the American Heart Association Statistics Committee and Stroke Statistics Subcommittee. Circulation. 115(5):e69-171. Epub 2006 Dec. 28.

Rosen J, Perry JC, Manning N, Burns S, Hannaford B. 2005. The human arm kinematics and dynamics during daily activities – towards a 7 DOF upper limb powered exoskeleton. Proceedings of the 12th International Conference on Advanced Robotics; July 18–20; Seattle, USA, pp. 532–539.

Sanchez RJ, Liu J, Rao S, Shah P, Smith R, Rahman T, Cramer SC, Bobrow JE, Reinkensmeyer DJ. 2006. Automating arm movement training following severe stroke: functional exercises with quantitative feedback in a gravity-reduced environment. IEEE Trans Neural Syst Rehabil Eng. 14(3):378–389.

Schiele A, van der Helm FCT. 2006. Kinematic design to improve ergonomics in human machine interaction. IEEE Trans Neural Syst Rehabil Eng. 14(4):456–469.

Soslowsky LJ, Flatow EL, Bigliani LU, Mow VC. 1992. Articular geometry of the glenohumeral joint. Clin Orthop Related Res. 285: 181–190.

Stienen AHA, Hekman EEG, Van der Helm FCT, Prange GB, Jannink MJA, Aalsma AMM, Van der Kooij H. 2007. Dampace: dynamic force-coordination trainer for the upper extremities. Proceedings of the IEEE 10th International Conference on Rehabilitation Robotics; June 13–15; Noordwijk, The Netherlands, pp. 820–826.

Sugar TG, He J, Koeneman EJ, Koeneman JB, Herman R, Huang H, Schultz RS, Herring DE, Wanberg J, Balasubramanian S, et al. 2007. Design and control of RUPERT: a device for robotic upper extremity repetitive therapy. IEEE Trans Neural Syst Rehabil Eng. 15(3):336–346.

Sunderland A, Tinson DJ, Bradley EL, Fletcher D, Langton HR, Wade DT. 1992. Enhanced physical therapy improves recovery of arm function after stroke: a randomised clinical trial. J Neurol Neursurg Psychiatr. 55:530–535.

Thorvaldsen P, Asplund K, Kuulasmaa K, Rajakangas AM, Schroll M. 1995. Stroke incidence, case fatality, and mortality in the WHO MONICA Project. Stroke 26:361–367.

van Andel CJ, Wolterbeek N, Doorenbosch CA, Veeger DH, Harlaar J. 2008. Complete 3D kinematics of upper extremity functional tasks. Gait Posture 27(1):120–127.

van der Helm FCT, Pronk GM. 1995. Three-dimensional recording and description of motions of the shoulder mechanism. J Biomech Eng. 117(1):27–40.

Volpe BT, Krebs HI, Hogan N. 2001. Is robot-aided sensorimotor training in stroke rehabilitation a realistic option? Curr Opin Neurol. 14(6):745–752.

Winter D. 1989. Biomechanics and motor control of human movement, 2nd. Edition. Wiley, New York, NY, USA.

Zatsiorsky VM. 1998. Kinematics of human motion, Champaign, IL: Human Kinetics.

Zhang LQ, Park HS, Ren Y. 2007. Developing an intelligent robotic arm for stroke rehabilitation. Proceedings of the IEEE 10th International Conference on Rehabilitation Robotics; June 12–15; Noordwijk, The Netherlands, pp.984–994.